Supporting Information *(Salter et al, photosynthetic induction kinetics in wheat)*

Appendix S1

A. Preliminary field measurements of photosynthetic induction kinetics

We measured photosynthetic induction kinetics in 58 genotypes of wheat. This preliminary study was a by-product of measurements of CO_2- and light-saturated net assimilation rate (A_{max}) for a related study. Because the workflow was organized around a broader phenotyping study (in which 160 genotypes were measured), replication was unbalanced among the 58 genotypes for which we recorded induction kinetics, with n = 1 to 4 replicate plants per genotype. As such, we do not base any conclusions on these kinetics results; instead, we suggest that these data should be viewed as preliminary results that hint at the occurrence of wide genetic variation in induction kinetics, and which motivated us to perform the more rigorous study described in the main text. We include these results here only for readers' interest.

A1. Plant material

Wheat was planted in 2 x 6 m plots with five sowing rows per plot in Narrabri, NSW, Australia in late May 2017. 58 genotypes were examined (Table S1). Measurements were made between 03 Sep 2017 and 18 Sep 2017, within two weeks before or after anthesis (the distribution of Zadoks phenological stages across the field measurement campaign is shown in Figure S1).

A2. Gas exchange system

We measured photosynthetic induction upon transition from darkness to saturating light in penultimate leaves using an open-flow single-pass differential gas exchange system with eight leaf chambers (5 × 11 cm) ("OCTOflux", described elsewhere; Salter *et al.*, 2018). OCTOflux was designed to maximize throughput for measurements of A_{max}. Each chamber has a white LED light source above the adaxial leaf surface, a Propafilm window, four small mixing fans and a type T thermocouple kept appressed to the abaxial surface. Stable dry air is created by mixing CO_2 and dry air from pressurized cylinders with mass flow controllers into a buffering volume (~40 L) containing a powerful fan. This gas is then split into nine streams: a reference stream, which flows through the reference cell of a differential infrared gas analyzer (IRGA; Li-7000, Li-Cor, Lincoln, Nebraska), and eight sample streams, each of which runs through a mass flow meter to a leaf chamber and back to the IRGA, where it is either vented to the atmosphere or directed through the IRGA sample cell, using solenoid valves.

A3. Measurement procedure

Tillers were cut in the field, immediately recut under distilled water and placed into darkness and transported by vehicle to the laboratory (about 1 km away; time from cutting to laboratory was 5-15 min), and kept in darkness for a further 0 – 30 minutes before measurement. Each leaf was enclosed in a leaf chamber and exposed to saturating PPFD (1700 μmol m^{-2} s^{-1}) and chamber CO_2 of 4800 – 5000 μmol mol^{-1}, and allowed to acclimate to these conditions. To verify that A_{max} measured at these high c_a values did not differ substantially from the true A_{max}, which occurs at the transition point between RuBP-regeneration-limited and triose phosphate utilization (TPU)-limited photosynthesis, we measured traditional A vs c_i curves in 18 leaves and extrapolated these to high c_a using a biochemical model (Farquhar *et al.*, 1980) as extended by Busch et al. (2018), and found that A_{max} at 5000 μmol mol^{-1} was an excellent proxy for true A_{max} (Fig S2); full details of these tests are given in Salter et al. (2018).

We recorded net CO_2 assimilation rate every two seconds until stability was achieved (average ~14 min), and the record of A vs time was then modeled with the following sigmoidal equation:

(S1) $$A(t) = A_{init} + \left(A_{\max} - A_{init}\right)\exp\left(-a \cdot \exp\left(-bt\right)\right)$$

where A_{init}, A_{max}, a and b are positive empirical parameters fitted by using Solver (GRG nonlinear engine) in Microsoft Excel to minimize the sum of squared differences between measured and modeled A. The times for A to rise by 25%, 75% and 95% of the difference between A_{init} and A_{max} (t_{25}, t_{75} and t_{95}, respectively) were then calculated from the fitted parameters, as $t_x = \ln(a/\ln(1/[0.01 \cdot x]))/b$, where x = 25, 75 or 95. The "rise time," or the time required for A to increase through the middle 50% of its dynamic range, was calculated as $t_{75} - t_{25}$.

A4. A_{max} induction kinetics results

A representative timecourse of A_{max} induction of field grown plants is shown in Fig S1. Equation S1 fitted the induction kinetics of A_{max} with median $r^2 > 0.99$. Within-genotype median t_{95} (the time for A_{max} to rise through 95% of its dynamic range) ranged from 8.4 to 23.7 min across genotypes (Fig S4). The within-genotype median for $t_{75} - t_{25}$ (the time required for A_{max} to increase through the middle 50% of its dynamic range) varied from 1.5 to 7.6 min (Fig S4). Differences among genotypes were not significant for either variable ($F(57,73) = 0.8$, $p = 0.81$ for t_{95}, and $F(57,73) = 0.94$, $p = 0.6$ for $t_{75} - t_{25}$). Across genotypes, A_{max} was unrelated to t_{95} , $t_{75} - t_{25}$, or t_{25} (Fig S5).

B. Modeling impact of induction kinetics on carbon gain

B1. Photosynthesis.

We simulated daily carbon gain in relation to the observed range of photosynthetic induction kinetics using a procedure based on that of Taylor and Long (2017) (TL17) and Retkute et al. (2018) (R18). Like TL17, we modeled the equilibrium value of leaf photosynthesis (A_{eq}, i.e., the value that would occur if induction were instantaneous) using Eqn 1 in the main text, using genotype-specific values for θ, ϕ and A_{sat} (Table S2; response curves shown in Fig S6). To simulate the typical decline in photosynthetic capacity in relation to cumulative leaf area index within a canopy, we reduced A_{sat} in proportion to the ratio of simulated daily PPFD at a given canopy position to that above the canopy. We computed A at 10-second intervals over a diurnal timecourse comprising alternating sunflecks and shadeflecks (further details on light modeling are given below). During sunflecks, we modeled the increase in A over time using Eqn 2 in the main text, adapted for A as shown in Eqn S2:

(S2) $$A(t) = A_i + \left(A_{eq} - A_i\right)\left\{f\left(1 - \exp\left(-\frac{t}{\tau_{fast}}\right)\right) + \left(1 - f\right)\left(1 - \exp\left(-\frac{t}{\tau_{slow}}\right)\right)\right\}$$

where A_i is the value of A at the start of the sunfleck, and f, τ_{fast} and τ_{slow} are genotype-median values given in Table S2. During shadeflecks, we assumed that A intantaneously dropped to the new (shaded) value of A_{eq}. To determine the initial value (A_i) at the start of the next sunfleck, we simulated the gradual deactivation in the "target value" of A in the same manner as for its induction during sunflecks, except that the kinetic parameters τ_{slow} and τ_{fast} were set to 5/3 of the values used during sunflecks; this was based on TL17's assumption that τ = 5 min [300 s] during shadeflecks for their study genotype, for which they had measured τ during sunflecks to be 3 min [180 s].

B2. Above-canopy light environment

We simulated the diurnal timecourse of PPFD for a target leaf as follows. First, following R18, we computed the beam (direct) PPFD incident on a surface, i_{beam}, and the diffuse irradiance above the canopy, i_{do}, as

(S3) $$i_{beam} = i_{\max} \alpha^{1/\sin\beta} \cos\eta$$

and

(S4) $$i_{do} = 0.5 i_{\max} \left(1 - \alpha^{1/\sin\beta}\right) \sin\beta$$

respectively, where i_{max} is the PPFD above the atmosphere (2600 μmol m^{-2} s^{-1}), α is atmospheric transmissivity (0.8), β is the solar elevation and η is the angle between the leaf normal and the solar beam. β is given by

(S5) $$\beta = \arcsin\left\{\sin\delta \cdot \sin\lambda + \cos\delta \cdot \cos\lambda \cdot \cos h\right\},$$

where δ is the solar declination, λ is the latitude and h is the hour angle. δ is given by

(S6) $$\delta = -23.5\cos\left(\left(d + 10\right)/365\right),$$

where d is the Julian day, and h is given by

(S7) $$h = \pi\left(t - t_{noon}\right)/12,$$

where t_{noon} is the time of solar noon (assumed to be 12) and t is the current time of day, both in hours. We used λ = -30° and d = 252, which correspond to the time and date of our field measurements in Narrabri, NSW, Australia. We computed cos$h$ as

(S8) $$\cos\eta = \left|\cos\beta \cdot \cos\beta_{leaf} \cos\left(\phi_{sun} - \phi_{leaf}\right) + \sin\beta \cdot \sin\beta_{leaf}\right|,$$

where β_{leaf} and ϕ_{leaf} are the elevation and azimuth angles of the leaf normal vector, respectively, and ϕ_{sun} is the azimuth angle of the sun, computed as

(S9) $$\phi_{sun} = \pm\arccos\left\{\left(\sin\delta \cdot \cos\lambda - \cos\delta \cdot \sin\lambda \cdot \cos h\right)/\cos\beta\right\},$$

with the positive value taken when $h > 0$ and the negative value when $h < 0$.

B3. PPFD for leaves within a canopy

Leaf PPFD during shadeflecks was equal to the diffuse irradiance at a cumulative leaf area index of L, given by $i_{do} \cdot \exp(-k_d \cdot L)$, where k_d is diffuse extinction coefficient (0.78; de Pury & Farquhar, 1997). PPFD during sunflecks was equal to the shadefleck value plus the beam irradiance, i_{beam}.

B4. Shadefleck and sunfleck lengths

We simulated alternating sunflecks and shadeflecks, with sunflecks having a fixed length of $t_{sunfleck}$ and shadeflecks a variable length $t_{shadefleck}$. Given that the probability of a given leaf segment being in a

sunfleck at any given time is equal to exp(-L/sinβ) (de Pury and Farquhar 1997), $t_{sunfleck}/(t_{sunfleck} + t_{shadefleck})$ = exp(-L/sinβ), which is solved to give $t_{shadefleck}$ as

(S10) $$t_{shadefleck} = t_{sunfleck}\left(\frac{1-\exp\left(-L/\sin\beta\right)}{\exp\left(-L/\sin\beta\right)}\right).$$

The shadefleck length is thus greater near the shoulders of the day, as solar elevation β decreases, and also at greater depths in the canopy (greater L).

B5. Leaf orientation and canopy position

We simulated a range of leaves, with varying β_{leaf}, ϕ_{leaf} and L. We used four values of L (0.25, 0.75, 1.5 and 3.0 m^2 m^{-2}). Preliminary results indicated that leaf orientation had quite weak influence on the effects of non-instantaneous photosynthetic induction kinetics on % loss of diurnal carbon gain. We thus computed an average for each canopy layer, assuming a spherical leaf angle distribution (as typical for wheat; ref), by Monte Carlo averaging. To sample the spherical angle distribution, we used Box-Muller transformations on uniform random deviates in [0,1) (generated using the function Rnd() in VBA) to generate normally distributed, zero-centered random value for 3D Cartesian coordinates x, y and z, representing the endpoints of an imaginary leaf normal vector, and then computed β_{leaf} as arccos($z/(x^2 + y^2 + z^2)^{0.5}$) and ϕ_{leaf} as arctan(y/x). Preliminary calculations found that the average thus computed converged fairly quickly, with layer-averaged % C loss fluctuating by less than approximately 1% of its mean value for sample sizes over 50 leaves, so we used n=50 samples for results shown in the main text.

Figure S7 illustrates representative timecourses of simulated PPFD and fraction of time spent in sunflecks (exp(-L/sinβ)) for horizontal leaves at two canopy depths (L = 0.25 and 1.5 m^2 m^{-2}). Figure S8 shows results for three representative leaf orientations (horizontal, vertical facing north/south and vertical facing east/west).

Table S1. List of genotypes used in this study. All genotypes were used in the field study of induction of photosynthetic capacity in penultimate leaves; genotypes #50, 51, 83, 88, 130, 150, 161, 192, 213 and 216 were used for intensive analysis of photosynthetic induction kinetics using dynamic *A* vs c_i curves in flag leaves.

number	designation
4	PBW502
7	MACE
15	PBI09C004-BC-DH24
16	PBI09C004-BC-DH74
21	PBI09C004-BC-DH118
25	PBI09C001-BC-DH9
32	PBI09C045-BC-DH15
39	PBI09C043-BC-DH28
43	PBI09C049-BC-DH5
44	PBI09C049-BC-DH6
45	PBI09C048-BC-DH11
50	PBI09C048-BC-DH36
51	PBI09C047-BC-0C-1N-99N
55	PBI09C035-BC-DH7
56	PBI09C035-BC-DH11
59	PBI09C035-BC-DH25
66	PBI09C034-BC-DH29
68	PBI09C034-BC-DH33
73	PBI09C034-BC-DH17
78	PBI09C038-BC-DH9
79	PBI09C038-BC-DH17
81	PBI09C038-BC-DH10
82	PBI09C038-BC-DH22
83	PBI09C038-BC-DH21
88	PBI09C039-BC-DH63
90	PBI09C010-BC-DH1
93	PBI09C010-BC-DH9
99	PBI09C008-BC-DH8
104	PBI09C008-BC-DH35
122	PBI09C028-BC-DH2
125	PBI09C028-BC-DH7
130	PBI09C028-BC-DH54
135	PBI09C026-BC-DH65

139	PBI09C026-BC-DH88
143	31 : ZWW10
147	238 : ZWB13
150	27 : ZIZ13
153	334 : ZWB13
161	ACIAR09PBI C04-23C-DH7
163	ACIAR09PBI C08-0C-0N-11N
164	ACIAR09PBI C06-0C-0N-2N
171	171 : ZWB13
176	35 : ZWB14
179	103 : ZWB14
180	142 : ZWB14
192	F946
193	F589
195	F1036
202	F1572
207	GREGORY
210	F808
213	F656
216	F1431
221	F1178
226	F1303
227	F1501
239	F907
241	F1265

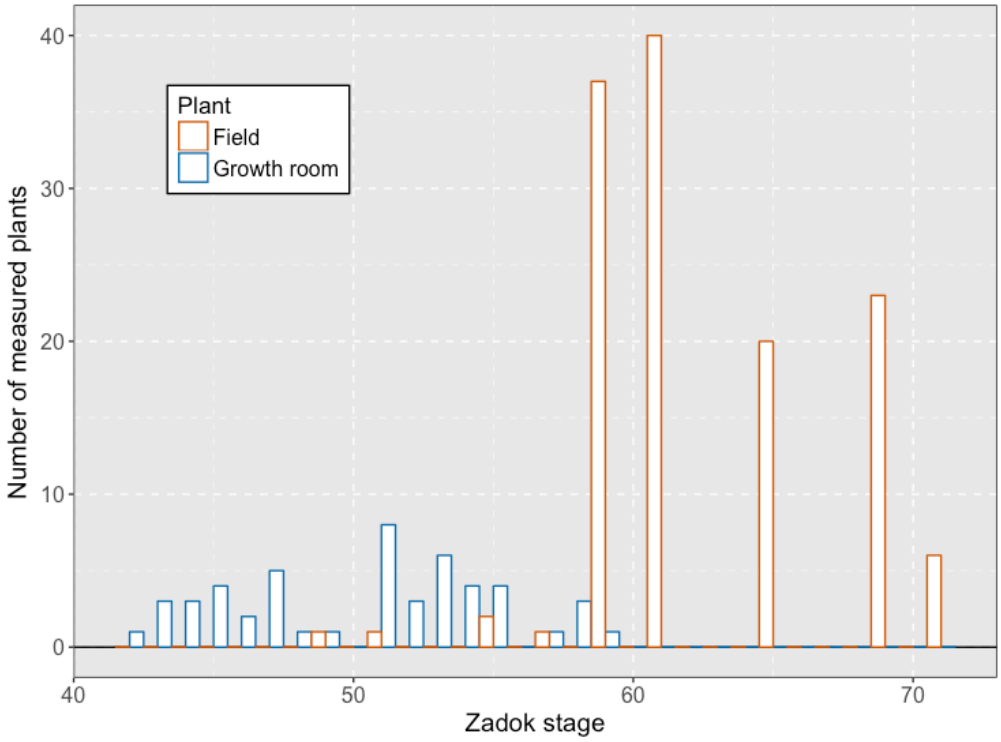

Figure S1. Distribution of phenological stages (Zadok stages) of plants measured in this study. Blue bars represent plants grown under controlled conditions, orange bars represent field grown plants.

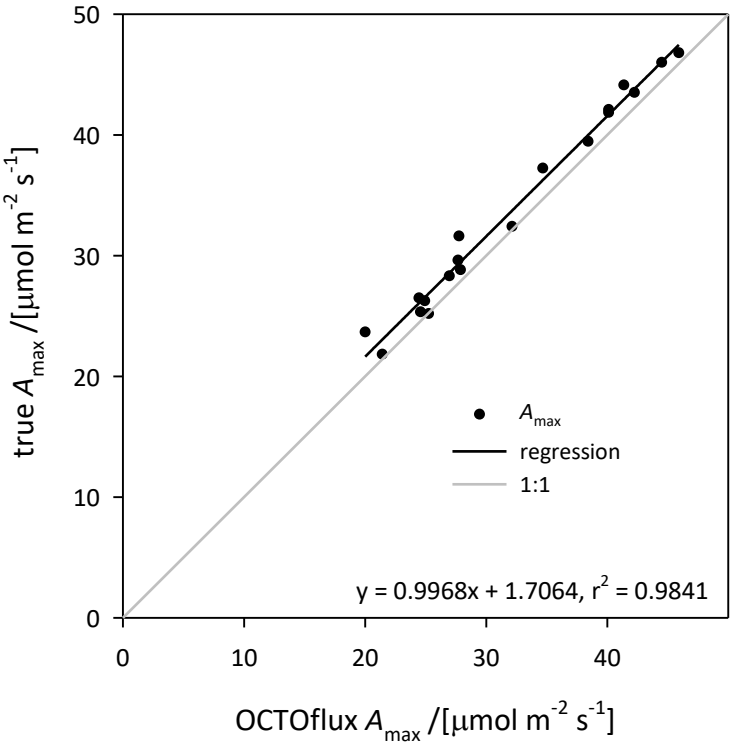

Figure S2. Relationship between true A_{max} (value at the transition from electron transport limited conditions to TPU limited conditions) and OCTOflux A_{max} (value at high CO_2 under TPU-limited conditions, estimated by extrapolating to high c_i the Busch et al. (2018) model for TPU-limited A fitted to A vs c_i curve data for 18 A vs c_i curves. Black line is a regression: $y = 0.9968 \cdot x + 1.7064$, $r^2 = 0.9841$, and grey line is 1:1.

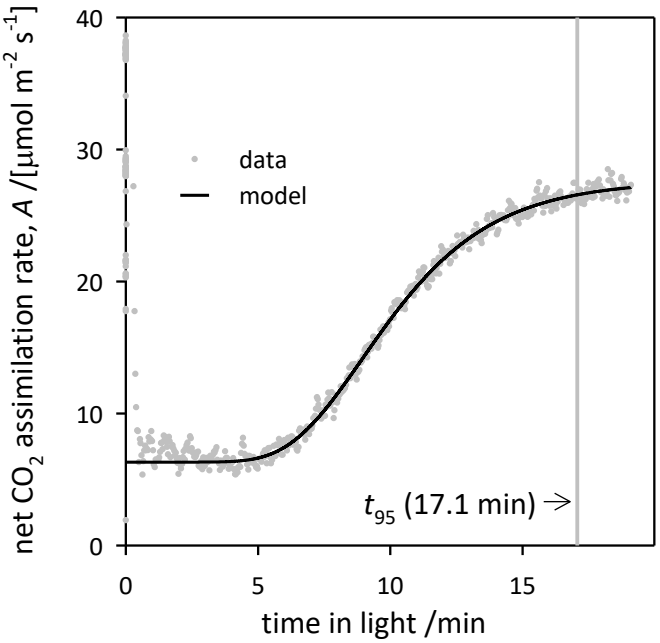

Figure S3. Representative time-course of CO_2- and light-saturated net assimilation rate measured in field-grown plants (A_{max}). The time at which A_{max} rose through 95% of its dynamic range (t_{95}) is shown with a vertical grey bar. Grey circles are data, and the solid black line indicates model fit (Eqn S1).

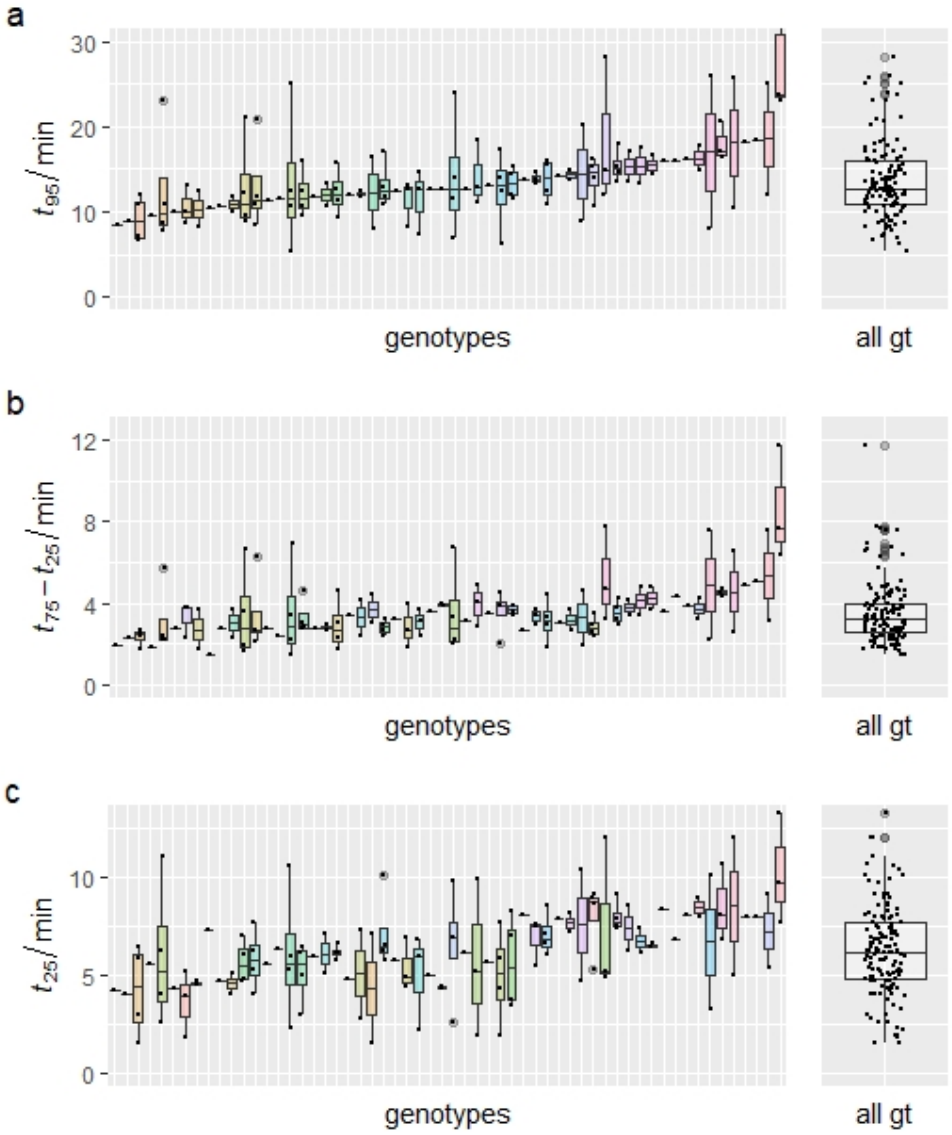

Figure S4. Distribution of values of (a) t_{95}, (b) t_{75} - t_{25}, and (c), t_{25}, the times for A_{max} to increase through 95% of its dynamic range (t_{95}), through the middle 50% of its dynamic range ($t_{75} - t_{25}$), or through the first 25% of its dynamic range (t_{25}). 58 genotypes were studied, of which 37 had 2-4 replicates. The center line in each box plot indicates the median, the upper and lower bounds of each box indicate the 75th and 25th percentiles, respectively, the whiskers indicate the 90th and 10th percentiles, respectively, and the black circles indicate individual values above or below the latter percentiles. Distributions for all genotypes combined are shown at right.

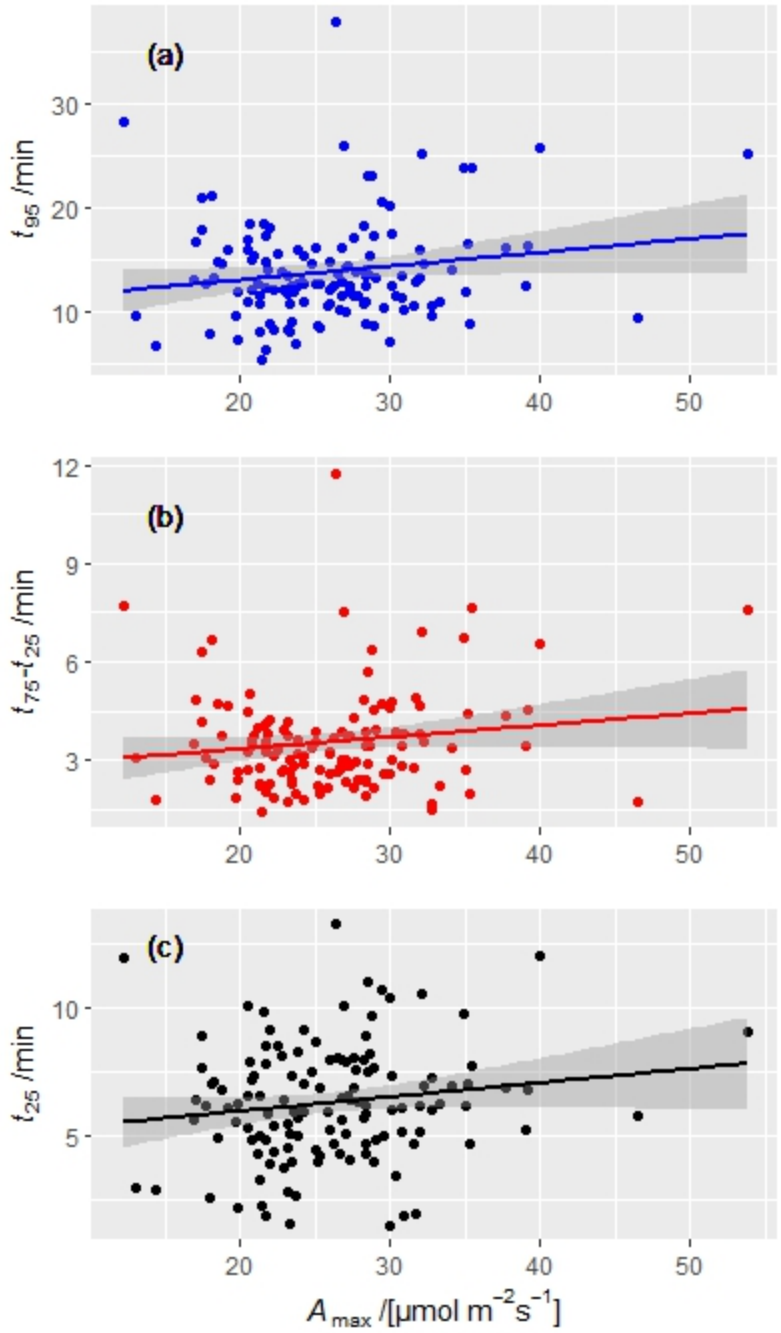

Figure S5. Relationships between final (saturated) values of A_{max} in field-grown plants and induction kinetics parameters: (a) t_{95}, (b) $t_{75} - t_{25}$, and (c) t_{25}. Solid lines are regressions (all n.s.) with 95% confidence intervals: (a) $y = 0.126x + 10.49$, $r^2 = 0.078$, $p = 0.068$; (b) $y = 0.0315x + 2.735$, $r^2 = 0.126$, $p = 0.14$; (c) $y = 0.055x + 4.87$, $r^2 = 0.041$, $p = 0.089$.

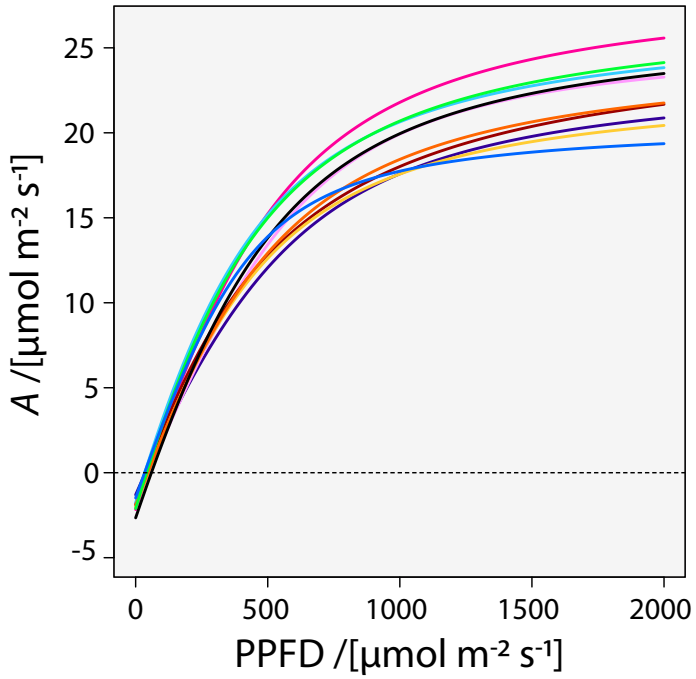

Figure S6. Fitted light response curves for the ten genotypes used in this study. Parameters for these curves are given in Table S2.

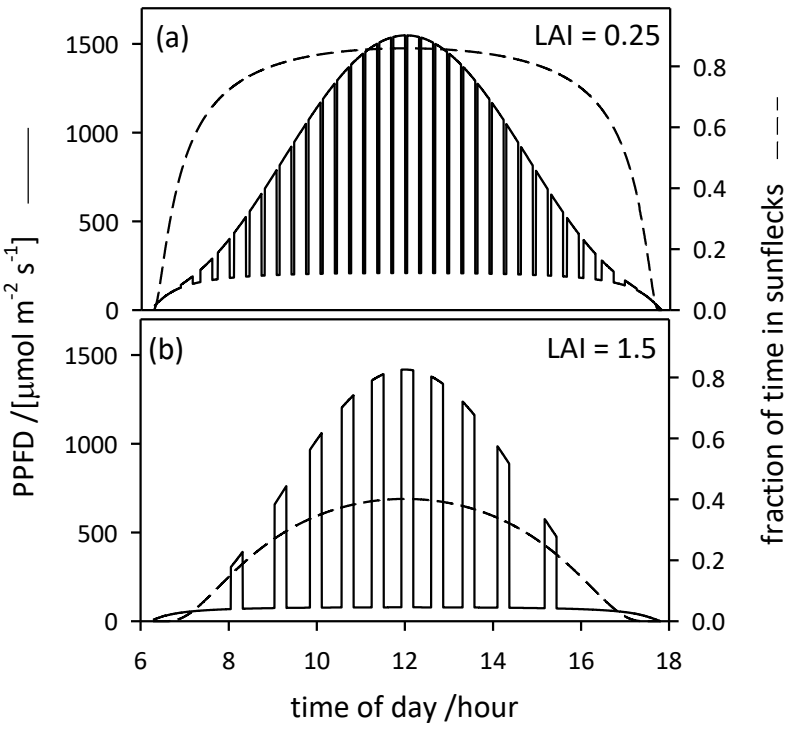

Figure S7. Representative time-courses of simulated PPFD with alternating sunflecks and shadeflecks (solid lines, left axis) and the fraction of time spent in sunflecks by leaves (dashed lines, right axis), for two canopy positions: cumulative leaf area indices of (a) 0.25 m^2 m^{-2}, and (b) 1.5 m^2 m^{-2}. Simulations assumed a constant sunfleck duration of 16 minutes.

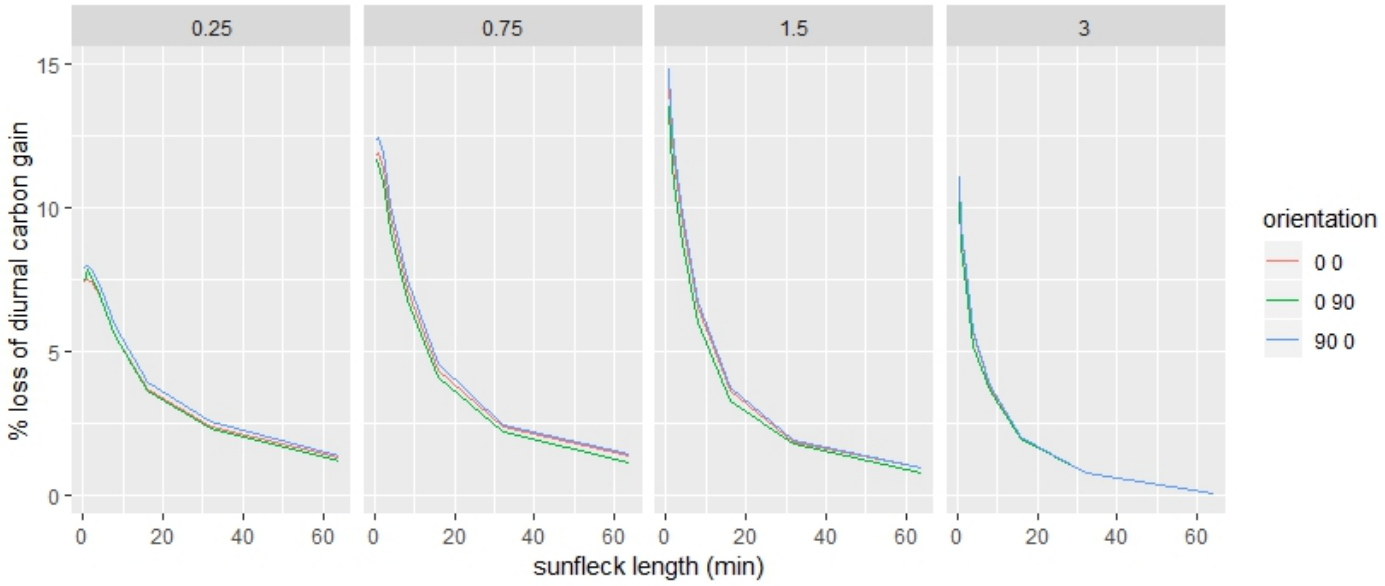

Figure S8. Effect of leaf orientation on simulated % loss of diurnal carbon gain, for a range of sunfleck durations (x axis), at four different canopy depths (indicated by the LAI values, in m^2 m^{-2}, given at the top of each panel). Within each panel, each line represents a different leaf orientation, indicated by the numbers in the legend at right (first number = elevation of leaf normal vector, in degrees; second number = azimuth of leaf normal vector). Simulations used average values across genotypes for the kinetic and photosynthetic light response parameters given in Table S2.

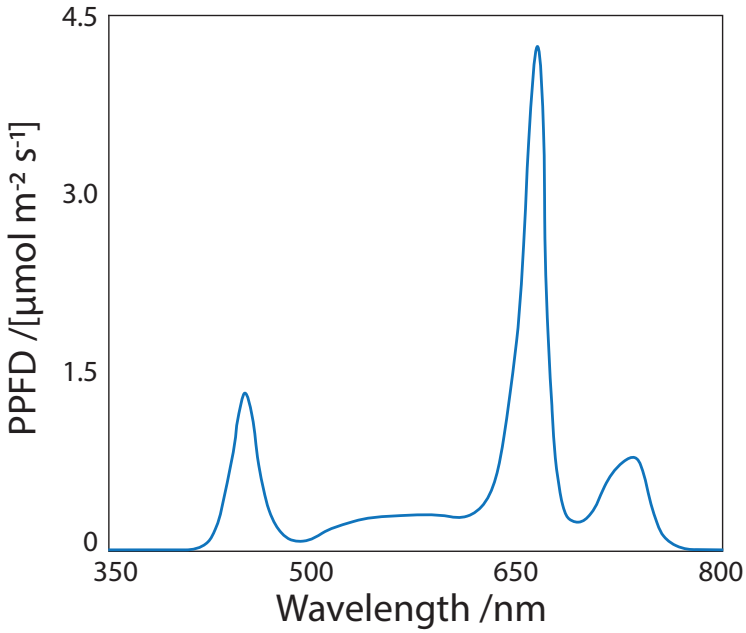

Figure S9. Spectral output of the controlled environment room LED growth lamps (LX602C; Heliospectra AB, Göteborg, Sweden), measured at a 2 m distance. Data obtained from Heliospectra.

References

Busch FA, Sage RF, Farquhar GD. 2018. Plants increase CO_2 uptake by assimilating nitrogen via the photorespiratory pathway. *Nature Plants* **4**(1): 46.

de Pury DGG, Farquhar GD. 1997. Simple scaling of photosynthesis from leaves to canopies without the errors of big-leaf models. *Plant, Cell and Environment* **20**: 537-557.

Farquhar GD, von Caemmerer S, Berry JA. 1980. A biochemical model of photosynthetic CO_2 assimilation in leaves of C_3 species. *Planta* **149**: 78-90.

Retkute R, Townsend AJ, Murchie EH, Jensen OE, Preston SP. 2018. Three-dimensional plant architecture and sunlit–shaded patterns: a stochastic model of light dynamics in canopies. *Annals of Botany*.

Salter WT, Gilbert ME, Buckley TN. 2018. A multiplexed gas exchange system for increased throughput of photosynthetic capacity measurements. *Plant Methods* **14**(1): 80.

Taylor SH, Long SP. 2017. Slow induction of photosynthesis on shade to sun transitions in wheat may cost at least 21% of productivity. *Philosophical Transactions of the Royal Society B* **372**(1730): 20160543.